JOURNAL OF QUATERNARY SCIENCE (2014) **29**(1) 41–56 ISSN 0267-8179. DOI: 10.1002/jqs.2674

Environmental changes in Baffin Bay during the Holocene based on the physical and magnetic properties of sediment cores

MARIE-PIER ST-ONGE[1,2]* and GUILLAUME ST-ONGE[1,2]
[1]Canada Research Chair in Marine Geology, Institut des sciences de la mer de Rimouski (ISMER), Université du Québec à Rimouski, Rimouski, Canada
[2]GEOTOP Research Center

Received 3 November 2012; Revised 27 September 2013; Accepted 15 October 2013

ABSTRACT: The physical and magnetic properties of four long sediment cores (HU2008-029-034PC, -038PC, -042PC and -070PC) sampled in Northern (Smith Sound and Jones Sound) and Eastern (Disko Bugt) Baffin Bay were analysed to reconstruct the Holocene environmental changes in Baffin Bay. Radiocarbon dating of each core revealed sedimentation rates of up to 136 cm ka^{-1}. Except for specific intervals, magnetic properties and ratios reveal that the magnetic remanence is mostly carried by magnetite and that changes in magnetic grain size and concentration are indicative of environmental variations associated with ice-rafted debris, sea-ice, meltwater pulses or terrigenous inputs. These variations indicate that all four cores, which cover a period from 12 360 cal a BP to the present, have sedimentary facies that correspond to the major climatic changes of the Holocene: deglaciation and the climatic optimum. In addition, two cores (HU2008-029-038PC and -070PC) present the signal of two climatic events with a local influence during the Neoglacial period. Copyright © 2013 John Wiley & Sons, Ltd.

KEYWORDS: Baffin Bay; deglaciation; Disko Bugt; Holocene; magnetic mineralogy; Neoglaciation; paleoceanography; sedimentology; western Greenland.

Introduction

The Baffin Bay region is a pathway for Arctic fresh waters and ice to the North Atlantic Ocean that play a crucial role in global oceanic circulation and climate (Holland *et al.*, 2001; Tang *et al.*, 2004). The modern pattern of circulation in the North Atlantic Ocean appeared during the Early Holocene, particularly with the opening of the Nares Strait in northernmost Baffin Bay at 9000 cal a BP (Jennings *et al.*, 2011). During the Holocene, the connection between the Arctic and Atlantic Oceans probably triggered local and global environmental changes, marked by associated sediment signatures (Miller *et al.*, 2005; Jennings *et al.*, 2011; Wanner *et al.*, 2011).

Further south, Disko Bugt is a key area for recording environmental changes associated with Greenland glaciers and changes in the West Greenland Current (WGC), which is a mixture of the warm Irminger current and the cold East Greenland current (Andersen, 1981; Tang *et al.*, 2004; Lloyd, 2006; Ribergaard *et al.*, 2008; Krawczyk *et al.*, 2010). Research on the influence of glaciers and ocean current variations upon sedimentation is crucial because it is very hard to find unequivocal evidence of the response of sea-ice margins to specific climatic changes (Lloyd, 2006; Ò Cofaigh *et al.*, 2013).

In this rich context of environmental complexity, paleoceanographic data from northern and southern Baffin Bay could be used to determine whether the Holocene climatic events were of local or regional extent (Jennings, 1993; Levac *et al.*, 2001; Knudsen *et al.*, 2008; Jennings *et al.*, 2011; Ò Cofaigh *et al.*, 2013). The physical and magnetic properties of marine sediments can record these changes at a high temporal resolution (Jennings, 1993; Francus, 2004; St-Onge *et al.*, 2007; Knudsen *et al.*, 2008).

In this paper, using the high-resolution physical and magnetic properties of four piston cores, we will describe and interpret the sedimentary units associated with environmental changes during the Holocene in northern Baffin Bay and offshore Disko Bugt. Our results provide a picture of the changes during the Holocene and highlight local particularities in the studied areas.

*Correspondence to: M.-P. St-Onge, as above.
E-mail: marie-pier.st-onge@uqar.ca

Geological and Environmental Setting

Baffin Bay is located between north-eastern Canada and western Greenland (Fig. 1). It is 450 km wide and 1300 km long (Aksu and Piper, 1987), and it connects the Arctic and North Atlantic Oceans via Nares Strait, Lancaster Sound and Jones Sound (Tang *et al.*, 2004). Sediment transport is affected by fresh meltwater flux from land, icebergs and seasonal pack ice (Holland *et al.*, 2001; Tang *et al.*, 2004; Perner *et al.*, 2011). The dominant current, consisting of cold Arctic water, flows from west to east in Jones Sound and from north to south in Smith Sound (Tang *et al.*, 2004). The northern part of Baffin Bay can provide important paleoclimate data due to the meeting of the WGC and polar waters from the Arctic Ocean (Tang *et al.*, 2004; Knudsen *et al.*, 2008).

Disko Bugt is a large marine embayment (Kelly and Lowell, 2009). The area is of particular interest because of the proximity of the Jakobshavn Isbrae ice stream, one of the fastest ice streams in the world (Lloyd, 2006) which drains ~6.5% of the Greenland Inland Ice (Weidick and Bennike, 2007).

Material and Methods

Coring sites and core handling

During the HU2008-029 oceanographic campaign in Baffin Bay, four piston cores (cores 034, 038, 042 and 070PC), with their companion trigger weight cores (TWC) and associated box cores (BC), were collected on board the CCGS *Hudson* (Fig. 1 and Table 1). Cores 034 and 038 were collected in the northern Baffin Bay polynya (Smith Sound). Core 042 was sampled in Jones Sound, whereas core 070 was raised offshore from Disko Bugt, north-west of Outer Egedesminde Dyb (valley) in a probable glacier outlet zone (Weidick and

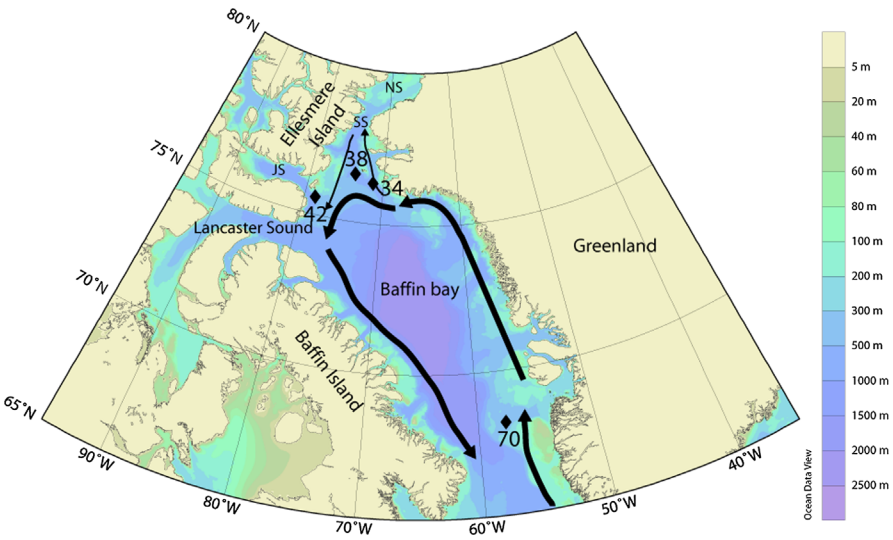

Figure 1. Map of Baffin Bay and the location of the four coring sites. The bathymetric base map is from Ocean Data View. Surface currents are based on Melling *et al.* (2001) and Tang *et al.* (2004). JS, Jones Sound; SS, Smith Sound; NS, Nares Strait. This figure is available in colour online at wileyonlinelibrary.com.

Table 1. Coordinates and properties of the coring sites.

Core	Latitude (°N)	Longitude (°W)	Location	Water depth (m)	Length (cm)	Composite corrected length (cm)
34	76.32905	71.418998	North water polynia	696	710	742
38	76.57349	73.955535	North water polynia	680	846	863
42	75.57939	78.629571	Jones Sound	580	1059	1112
70	68.22788	57.61746	Off Disko Bugt	444	250	431

Bennike, 2007; Ò Cofaigh *et al.*, 2013; Figs 1 and 2 and Table 1). The coring sites were determined using a Knudsen 3.5-kHz chirp sub-bottom profiler to identify areas of thick apparent Holocene sequences with the absence of mass movements and/or sediment perturbations. Composite depths have been established (see the core top correlation section), and the composite cores (comprising the BC, TWC, and PC records) are referred to as cores 34, 38, 42 and 70 hereafter.

Once on board, the cores were cut into 1.5-m-long sections and split lengthwise. They were then described and sampled with u-channels, rigid u-shaped plastic liners of 1.5 m length and a 2 × 2-cm cross-section.

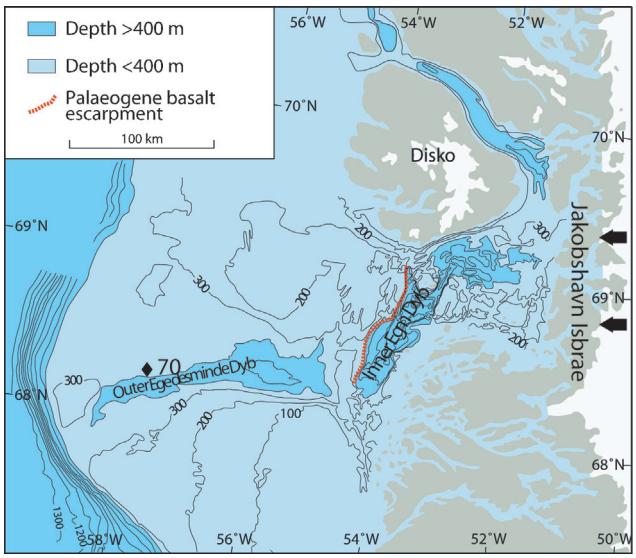

Figure 2. The continental shelf offshore Disko Bugt and the sampling location of core 70. From Weidick and Bennike (2007). This figure is available in colour online at wileyonlinelibrary.com.

Wet bulk density and low-field volumetric magnetic susceptibility

Wet bulk density and low-field volumetric magnetic susceptibility (k_{LF}) were first measured on board at 1- and 0.5-cm intervals, respectively, on whole piston, trigger weight and box cores using a GEOTEK Multi Sensor Core Logger. k_{LF} was also measured on u-channels in the laboratory at 1-cm intervals using a point sensor. k_{LF} is an indicator of the concentration of ferrimagnetic material and is sensitive to variations in grain size (e.g. Thompson and Oldfield, 1986; Stoner *et al.*, 1996; Dearing, 1999).

Diffuse spectral reflectance

Diffuse spectral reflectance was measured on board using a Minolta CM-2600d spectrophotometer at 0.5-cm intervals for the box and trigger weight cores and at 1-cm intervals for the piston cores. The spectral reflectance data are expressed in the CIE (International Commission on Illumination) L*, a*, b* color space which is often used in paleoceanography. L* ranges from black to white, a* from green to red, and b* from blue to yellow (e.g. St-Onge *et al.*, 2007). The L*, a*, b* data are smoothed to enhance the variations.

Grain size

Grain size measurements (0.04–2000 μm) were performed at 10-cm intervals in each core with a Beckman-Coulter LS13320 laser diffraction particle size analyser at ISMER. The top and bottom of each core section were also measured. Prior to the measurements, sediments were added to a Calgon electrolytic solution (sodium hexametaphosphate) and rotated for about 3 h using an in-house rotator. The samples were then sieved (2 mm) and disaggregated in an ultrasonic bath for 90 s before analysis. The particle size distribution output was then processed using the Gradistat software for sediment parameters (Blott and Pye, 2001).

CAT-scan

All core sections were passed through a computerized axial tomography scanner (CAT-Scan) at INRS-ETE in Quebec City to characterize the sedimentary facies and sediment structures (e.g. St-Onge *et al.*, 2007). It was notably used to determine the different sediment units, as well as to identify sediment deformation and shells for radiocarbon dating (see below).

Paleomagnetic analyses

All measurements were made at the Sedimentary Paleomagnetism and Marine Geology Laboratory of ISMER. Paleomagnetic data were measured on the u-channels at 1-cm intervals using a 2G Enterprises SRM-755 u-channel cryogenic magnetometer and pulse magnetizer module for isothermal (IRM) and saturated isothermal remanent magnetizations (SIRM). Because of the response function of the magnetometer (e.g. Weeks *et al.*, 1993; Roberts, 2006), smoothing occurs due to the integration of empty space at the end and beginning of u-channels. The first and the last 4 cm of each section were thus excluded.

The natural remanent magnetization (NRM) was measured and then progressively demagnetized using stepwise peak alternating fields (AFs) up to 80 mT at 5-mT increments. An anhysteretic remanent magnetization (ARM) was then induced using a 100-mT AF with a 0.05-mT direct current (DC) biasing field. The ARM was measured and demagnetized at every 5 mT up to 60 mT, and then at 70, 80, 90 and 100 mT. Two IRMs were imparted with a DC field of 0.3 T (IRM) and 0.95 T (SIRM) using the pulse magnetizer module. Each IRM was demagnetized and measured at peak AF at every 5 mT up to 60 mT, and at 70, 80, 90 and 100 mT. SIRM was demagnetized and measured at 0, 10, 30, 50, 70, 90 and 120 mT.

The median destructive field (MDF_{NRM}) of the NRM is also presented. It is the value of the AF necessary to reduce the NRM to half of its initial intensity and was calculated with the software from Mazaud (2005). MDF values are dependent on the coercivity of magnetic minerals and magnetic grain size, and are a useful parameter in estimating magnetic mineralogy (e.g. Dankers, 1981). The ARM_{20mT}/ARM_{0mT} ratio, a coercivity ratio that reflects variations in magnetic grain size if the mineralogy is dominated by low-coercivity minerals such as magnetite (e.g. Andrews *et al.*, 2003) was also calculated.

Additionally, the pseudo-S ratio ($IRM_{10mT}/SIRM_{10mT}$) was calculated to estimate the magnetic mineralogy, with values close to 1 indicating a lower coercivity, ferrimagnetic mineralogy (e.g. magnetite), and lower values indicating a higher coercivity mineralogy (e.g. hematite) (Stoner and St-Onge, 2007).

Hysteresis measurements were performed on selected sediment samples in each core using a Princeton Measurement Corporation (Princeton, NJ, USA) Micromag 2900 alternating gradient force magnetometer. Derived from the hysteresis curves, the coercivity of magnetic minerals (Hc), the coercivity of remanence (Hcr), the saturation magnetization (Ms) and the saturation remanence (Mrs) were used to characterize the magnetic mineralogy and grain size (Day *et al.*, 1977).

Radiocarbon dating

The chronologies of the composite sequences of cores 34, 38 and 42 were determined using accelerator mass spectrometry (AMS) ^{14}C measurements at the Keck carbon cycle AMS facility, University of California, Irvine, CA, USA. The measurements on box core 40, which is associated with core 42, were conducted at the Lawrence Livermore National Laboratory, Livermore, CA, USA. Radiocarbon measurements for core 70 samples were done at the NSF-Arizona AMS Facility and the Scottish Universities Environmental Research Centre in the UK (Jennings *et al.*, 2013). Detailed data are presented in Table 2. The ages are reported in radiocarbon years using Libby's half-life of 5568 years and following the convention of Stuiver and Polach (1977). The conversion of conventional ^{14}C ages to calibrated years was done using the CALIB 6.0 online calibration software (Stuiver *et al.*, 2005) and the Hughen *et al.* (2004) marine dataset. The regional reservoir corrections (ΔR values) used are indicated in Table 2 and based on the online CALIB marine reservoir correction database. The calibrated ages are the median probability reported with a 2σ confidence level.

Core top correlation

Physical and magnetic properties were correlated between the piston cores and their associated trigger weight and box cores to determine the amount of sediment loss during piston coring (Fig. 3). Composite depths were then constructed for each site using the determined sediment loss. Diffuse spectral reflectance (a^*) and magnetic susceptibility were used to compare the BC, TWC and PC of core 34. The correlation indicates a gap of 2 cm between the BC and TWC, and 34 cm between the TWC and PC. There is only a 4-cm gap between the BC and TWC of core 38, as shown by the inclination and k_{LF} data, whereas a difference of 19 cm between the TWC and PC is indicated by a^* and k_{LF} data. For core 42, a^* values indicate that there was 57 cm of sediments missing at the top of the piston core. Inclination and declination data were used to compare the BC, TWC and PC of core 70. Comparisons show that 15 cm of sediment is missing at the top of the TWC and that there is a difference of 161 cm between the TWC and PC. Comparison of foraminifera assemblages yielded similar results, i.e. 161 cm between TWC and PC (Jennings and Walton, 2010; Jennings *et al.*, 2013). The corrected lengths of all cores are presented in Table 1.

Results

Magnetic mineralogy and grain size

The shape of hysteresis curves of the discrete samples from all cores (Fig. 4) indicate that low-coercivity minerals such as magnetite in the pseudo-single domain (PSD) to multi-domain (MD) ranges are the dominant magnetic carrier (e.g. Tauxe, 2010). Similarly, Day plots (Day *et al.*, 1977) indicate that most of the sediments of the four cores are composed of PSD magnetic grains, except for core 38 which contains coarser MD magnetic grains (Fig. 5B). Mrs/Ms values ranging between 0.1 and 0.3 are characteristic of magnetite/titanomagnetite grains (Day *et al.*, 1977; Tauxe, 1993). Similarly, Hcr/Hc values ranging from 2 to 6 are typical of PSD to MD grain size for magnetite (Dunlop, 2002). Moreover, results from Day plot of cores 34, 42 and 70 follow a mixing line typical of magnetite/titanomagnetite grain size variations (Peters and Dekkers, 2003), whereas more scatter is observed for core 38. The k_{LF}/SIRM diagram indicates that for most of cores 34, 42 and 70, there is a scattered distribution of magnetic grain sizes, including larger MD grains in cores 34 and 70 (Fig. 5A–C). For core 34, this highlighted interval corresponds to 110–300 cm, but does not include the peak in MDF values between 204 and 181 cm. It is not related to a specific lithofacies, but it can be associated with low (<0.6) ARM_{20mT}/ARM_{0mt} values. Regarding core 70, this interval of MD grains ranges from 424 to 310 cm. It is related to a decrease in magnetic parameter values from 390 to 292 cm, and to the presence of coarser sediment in unit 1 (see below;

Table 2. Radiocarbon ages. The numbers in parentheses represent the lower and the upper limits of the two sigma error range.

Cores HU2008-029	Section	Depth (cm)	Corrected depth U-channel (cm)	Dated material	Lab no.	AMS age (^{14}C a BP)	ΔR	Calibrated age (cal a BP)
34PC	DE	157	187	Pelecypod fragments	UCIAMS-61330	4265	171 ± 23	4140 (4048–4220)
34PC	CD	280	304	Gastropod	UCIAMS-61331	5555	171 ± 23	5755 (5657–5840)
38TWC	AB	167	180	Entire pelecypod shell	UCIAMS-61337	2585	171 ± 23	2050 (1972–2126)
38PC	EF	195	212	Pelecypod fragments	UCIAMS-61333	3490	171 ± 23	3178 (3073–3260)
38PC	DE	253	263	Entire pelecypod shell	UCIAMS-61335	3875	171 ± 23	3621 (3546–3696)
38PC	CD	509	513	Pelecypod	UCIAMS-61340	5000	171 ± 23	5133 (5028–5247)
38PC	CD	528	532	Pelecypod	UCIAMS-61339	5075	171 ± 23	5251 (5122–5305)
38PC	CD	543	547	Shell fragments	UCIAMS-61338	5115	171 ± 23	5285 (5221–5366)
38PC	BC	586	587	Pelecypod fragments	UCIAMS-61341	5480	171 ± 23	5661 (5595–5723)
38PC	AB	740	734	Shell fragments	UCIAMS-61343	6425	171 ± 23	6702 (6636–6774)
38PC	AB	801	795	Shell fragments	UCIAMS-61342	7110	171 ± 23	7447 (7395–7509)
40BC	Box core	24	24	Shell fragments	CAMS-150983	810	252 ± 29	195 (95–277)
40BC	Box core	42	42	Shell fragments	CAMS-150984	975	252 ± 29	366 (290–442)
42PC	DE	547	598	Shell fragments	UCIAMS-61336	6305	252 ± 29	6468 (6397–6547)
42PC	DE	571	622	Pelecypod valve	UCIAMS-61334	6505	252 ± 29	6701 (6635–6773)
42PC	BC	766	810	Pelecypod	UCIAMS-61332	8155	252 ± 29	8367 (8317–8413)
70TWC	BC	82–83	97	Single valve *Arca glacialis*	AA84708	3197	140 ± 30	2828 (2754–2876)
70TWC	BC	97–98	112	Paired *Thyasira gouldi*	AA84709	3252	140 ± 30	2889 (2817–2953)
70TWC	AB	134–135	149	Seaweed	SUERC25670	5913	140 ± 30	6199 (6157–6266)
70TWC	AB	172	187	Paired *Macoma calcarea*	AA84710	7898	140 ± 30	8231 (8166–8302)
70TWC	AB	194–195	210	Seaweed	SUERC-3058	8464	140 ± 30	8891 (8838–8984)
70PC	BC	14–15	190	Seaweed	SUERC25672	7501	140 ± 30	7827 (7776–7900)
70PC	BC	55–56	213	Shell fragments	SUERC-3059	8830	140 ± 30	9368 (9309–9429)
70PC	AB	142–144.5	318	Fragments paired shell	AA84711	9831	140 ± 30	10 551 (10 502–10 592)
70PC	AB	169–170	345	Paired small *Macoma crassula*	AA84712	10190	140 ± 30	10 985 (10 773–11 191)
70PC	AB	188–189	364	Paired *Macoma calcalera*	AA84713	10174	140 ± 30	11 038 (11 001–11 137)
70PC	AB	209–211	385	Large paired *Macoma calcalera*	AA84714	10545	140 ± 30	11 478 (11 471–11 628)

417–375 cm, Fig. 5). In addition, the pseudo S-ratio in cores 42 and 70, with mean values of 0.96 and 0.94, suggests that magnetite is the dominant magnetic carrier. Cores 34 and 38, which are located in the North Water Polynya, have lower pseudo S-ratio mean values of 0.84 and 0.91, respectively. If the same ratio is used but at 0 mT, the ratios are higher with mean values of 0.89 and 0.95 for cores 34 and 38, respectively, again indicative of a dominance of low-coercivity minerals such as magnetite. However, for core 38, these relatively lower values in conjunction with scattered results on the Day plot (Peters and Dekkers, 2003) may indicate a minor contribution of higher coercivity minerals such as goethite.

The MDF for cores 34, 38, 42 and 70 ranges from 5 to 30 mT, 5 to 20 mT, 5 to 30 mT and 5 to 10 mT, respectively. These relatively low MDF values, in conjunction with pseudo S-ratios and hysteresis loops indicative of magnetite, suggest that the sediment has a low coercivity probably due to coarser magnetic grain sizes. Similar lower MDF values were also observed in the Chukchi Sea and were associated with coarser grains of magnetite (Lisé-Pronovost *et al.*, 2009). In brief, these data indicate that, excluding the specific intervals discussed above, the magnetic remanence is probably dominantly carried by low-coercivity minerals such as magnetite in the PSD range. Nonetheless, in some intervals and for the most part of core 38, MD grains are observed.

Stratigraphy, physical and magnetic properties

Core 34

The physical and magnetic properties of core 34 allowed the identification of two distinct stratigraphic units (Fig. 5A). Unit 1, from 715 to 560 cm, is composed of a sequence characterized by two layers of reddish brown sandy mud with pebbles and gravel. The coarser material present in both layers is reflected by higher density and magnetic susceptibility values, and is visible on the CAT-scan images. Two peaks of magnetic susceptibility, with values reaching 200×10^{-5} SI, are observed and represent two distinct sub-units: 1a and 1b. The first magnetic susceptibility peak in sub-unit 1a, around 615 cm, is coeval with the presence of few pebbles. The second sub-unit (1b: 715–640 cm), highlighted by a peak in L* and a* values, is a dense and compact reddish layer with laminations, sand, gravel and pebbles. Also, corresponding low inclination values indicate that this unit may be reflecting a rapidly deposited layer (Fig. 4A; e.g. St-Onge et al., 2004, 2012).

Unit 2, from 560 cm to the top of the core, is composed of olive-grey (5Y4/2) and dark olive-grey (5Y3/2) silty clays. This unit is divided in four sub-units based on the presence of shell fragments and traces of bioturbation in sub-units a and c. An increase in MDF and ARM_{20mT}/ARM_{0mT} is observed from 110 cm to the top of the unit, indicating a decrease in magnetite grain size (e.g. Andrews *et al.*, 2003; Stoner and St-Onge, 2007), as no significant change in magnetic mineralogy can be deduced from the hysteresis loops and IRM/SIRM (Figs 4 and 5).

Core 38

Core 38 is composed of olive-grey (5Y4/2) and dark olive-grey (5Y3/2) silty clays (Fig. 5B). Except for two peaks at 483 and 110 cm, MDF values are low (mean of 4.62 mT) and constant, suggesting a uniform mineralogy with a combination of low-coercivity and coarse magnetic grains. Two main stratigraphic units were distinguished.

The first unit, from 860 to 505 cm, is characterized by an increase in magnetic susceptibility and density and by the presence of numerous shell fragments and traces of bioturbation (see background dataset in Supporting information, Figs

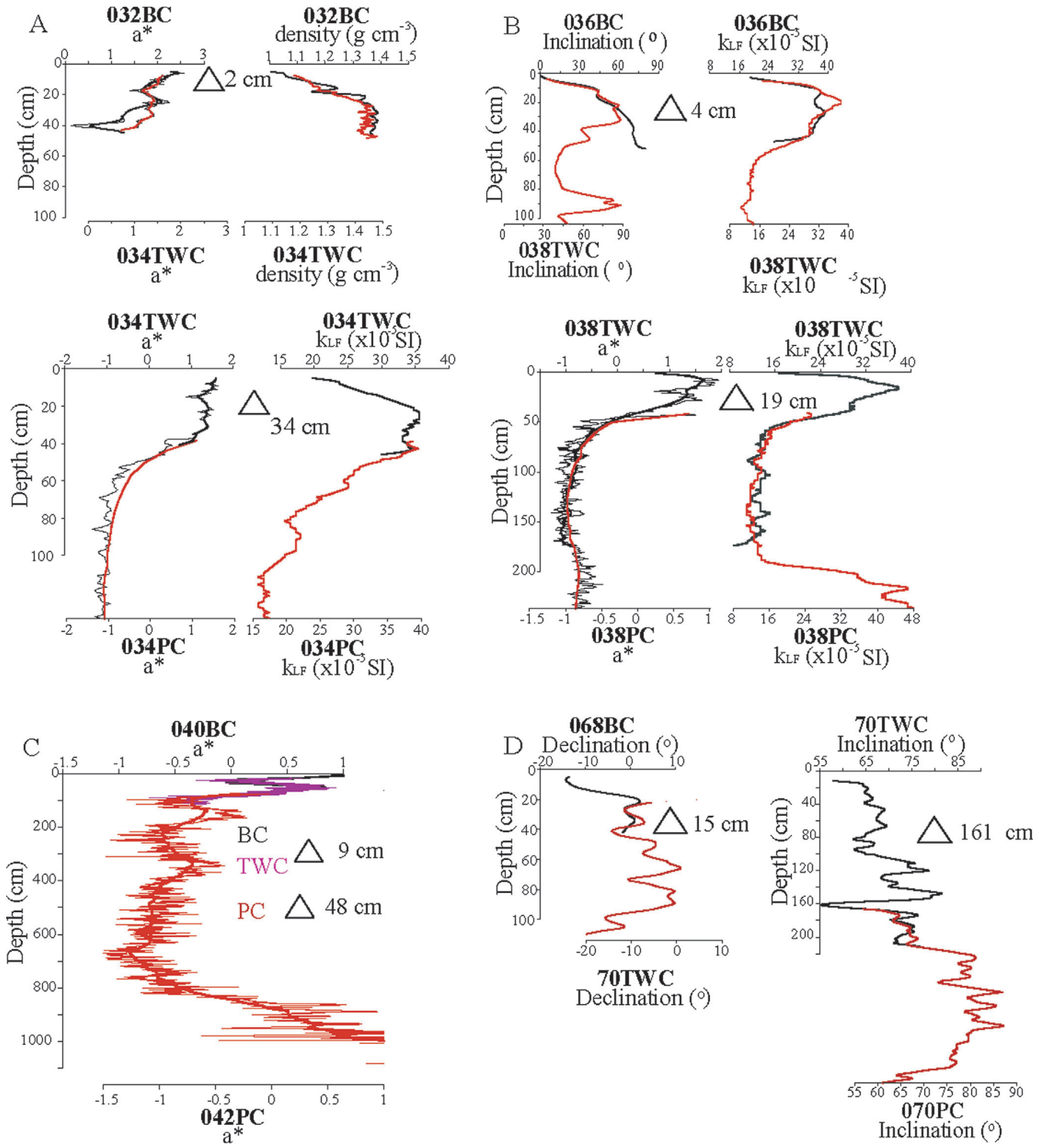

Figure 3. Core top correlation for cores (A) 32BC, 34TWC and 34PC, (B) 40BC and 42PC, (C) 36BC, 38TWC and 38PC, and (D) 68BC, 70TWC and 70PC. Open delta symbol represents the difference between each core. Colors illustrate the different sections. This figure is available in colour online at wileyonlinelibrary.com.

S1 and S2). Note that all the properties of this unit are constrained in the same range of values as sub-units 2a, 2b and 2c of core 34, possibly indicating a similar source and mode of deposition.

The second unit, from 505 cm to top of the unit, is characterized by the absence of significant traces of bioturbation or color changes and constant parameters. Sub-units a and c are very similar. Sub-unit 2b contains some pebbles and shell fragments. Higher values of magnetic susceptibility, from 280 to 180 cm, are apparent and reach a maximum of 52×10^{-5} SI. The higher density and coarser physical grain size observed in this sub-unit, in conjunction with lower values of ARM_{20mT}/ARM_{0mT}, indicate a coarser magnetic grain size (e.g. Andrews *et al.*, 2003; Stoner and St-Onge, 2007) as no significant change in magnetic mineralogy can be deduced from the hysteresis loops and IRM/SIRM ratio (Figs 4 and 5).

Core 42

Most of core 42 is composed of olive-grey (5Y4/2) and dark olive-grey (5Y3/2) silty clays with a gradual color change to very dark brown (10YR2/2) starting at 980 cm. Two stratigraphic units were defined.

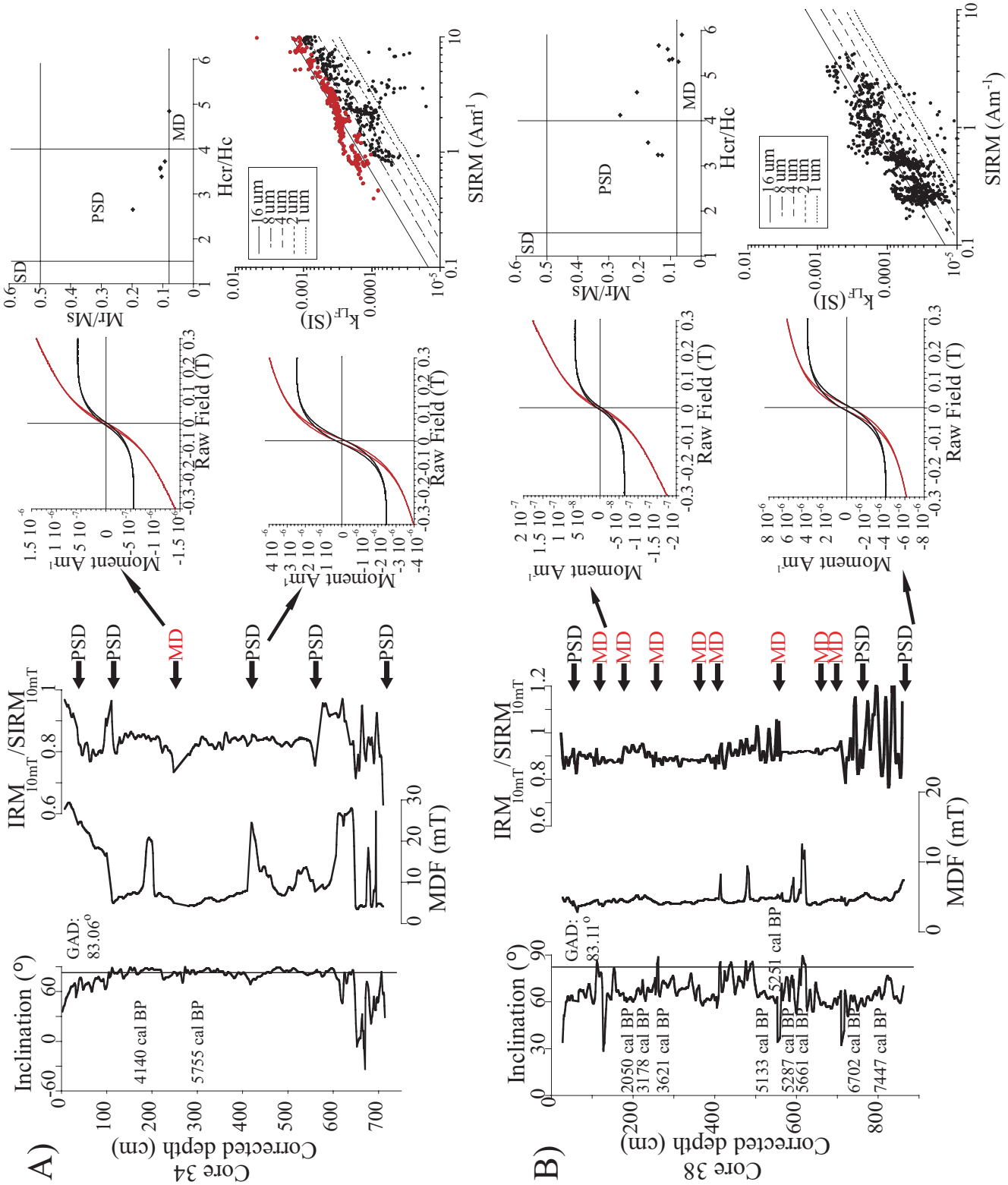

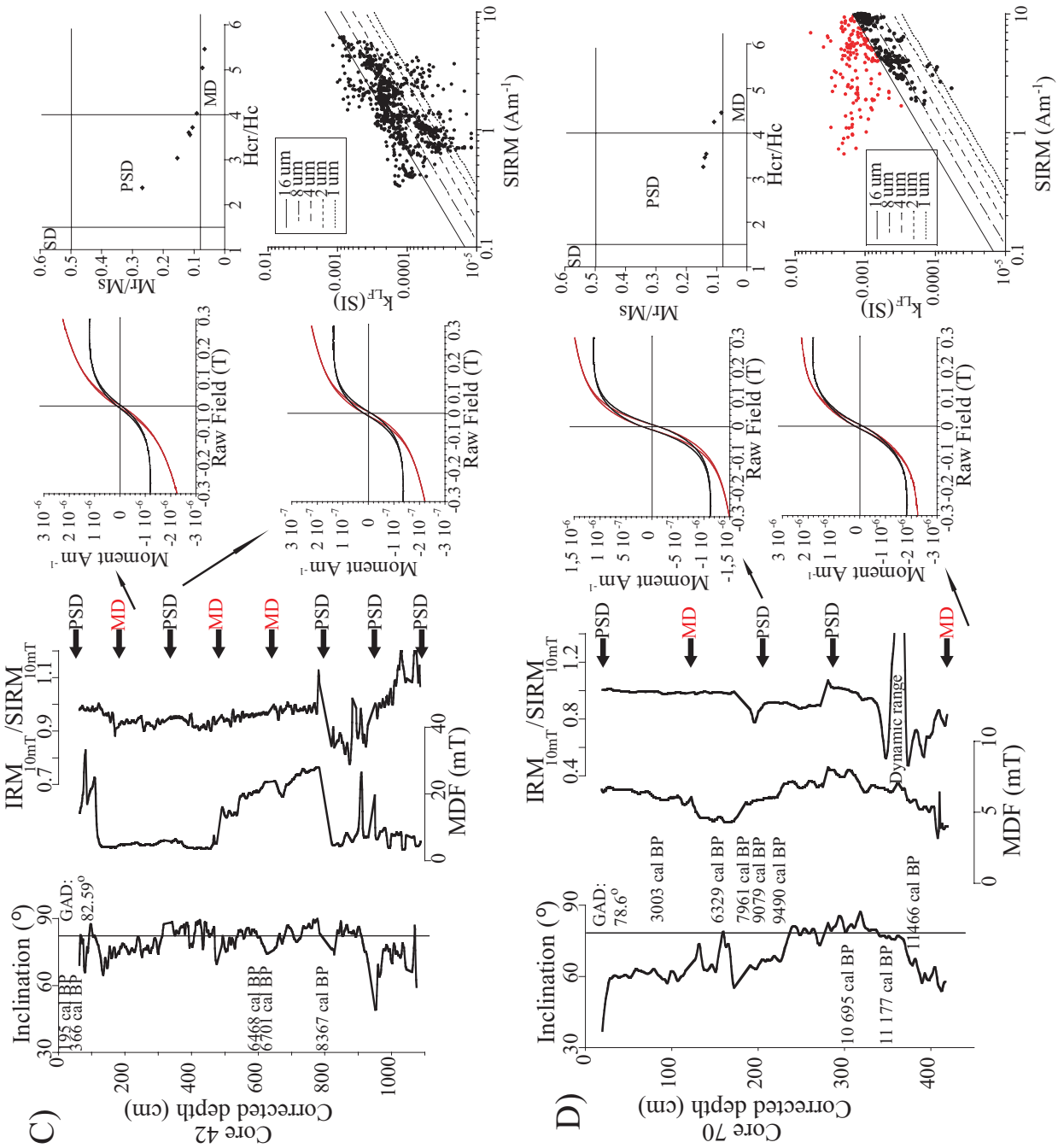

Figure 4. Downcore variations of the MDF, pseudo S-ratio and magnetic grain size indicator SIRM versus k_{LF} for cores (A) 34, (B) 38, (C) 42 and (D) 70. The magnetic grain size measurements are also represented in a Day plot (Day *et al.*, 1977) with their associated hysteresis curves. The arrows indicate where the u-channels were sub-sampled for the alternating gradient force magnetometer (AGM) measurements. The raw (red) and high-field slope corrected (black) magnetizations are illustrated. Red dots in the Day plots are associated with MD grains. MD, multi-domain; PSD, pseudo-single domain. The magnetic grain size trending lines in the k_{LF} vs SIRM diagrams are from Thompson and Oldfield, 1986. This figure is available in colour online at wileyonlinelibrary.com.

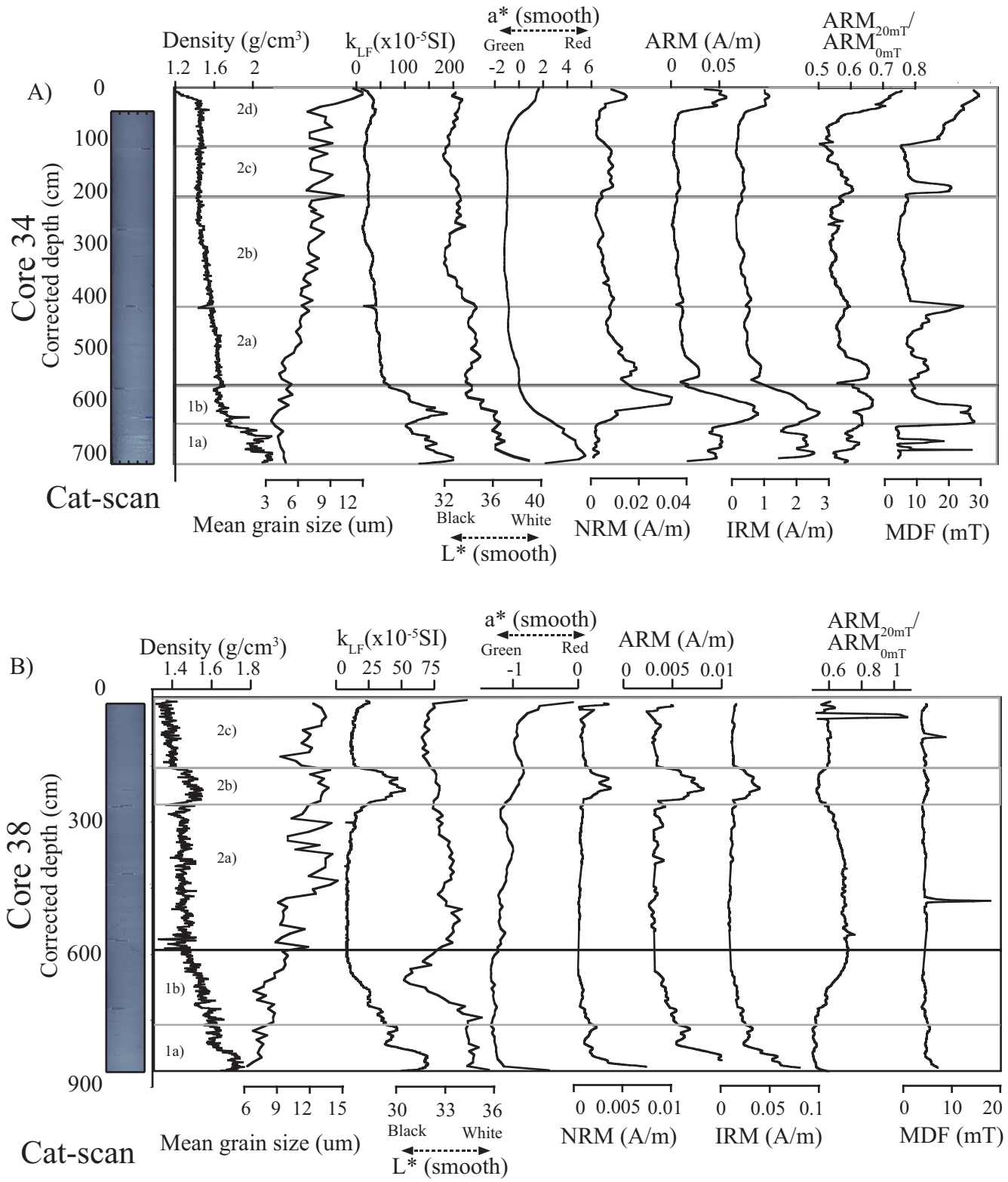

Figure 5. Downcore physical and magnetic properties with CT-Scan images for core (A) 34, (B) 38, (C) 42 and (D) 70. This figure is available in colour online at wileyonlinelibrary.com.

Unit 1 is observed from 1087 to 835 cm. It is defined by a significant color change from the base to the top of the unit, passing from a* values of +2 to −1. The succession of peaks in magnetic susceptibility, NRM, ARM and IRM profiles indicates that deposition occurred in several steps. Peaks observed only in magnetic susceptibility data at 1080, 1000 and 845 cm are associated with large pebbles that were not sampled in u-channels, but measured on the whole core analysis. High magnetic susceptibility, NRM, ARM and IRM values between 950 and 880 cm are related to small pebbles present in the u-channels.

The unit has been divided in two sub-units. Sub-unit 1a, from 1087 to 1068 cm, is composed of compact clay with large pebbles. Sub-unit 1b, from 1068 to 835 cm, is characterized by the presence of numerous pebbles in a very dark brown silty clay with layers of sandy mud. There are a few

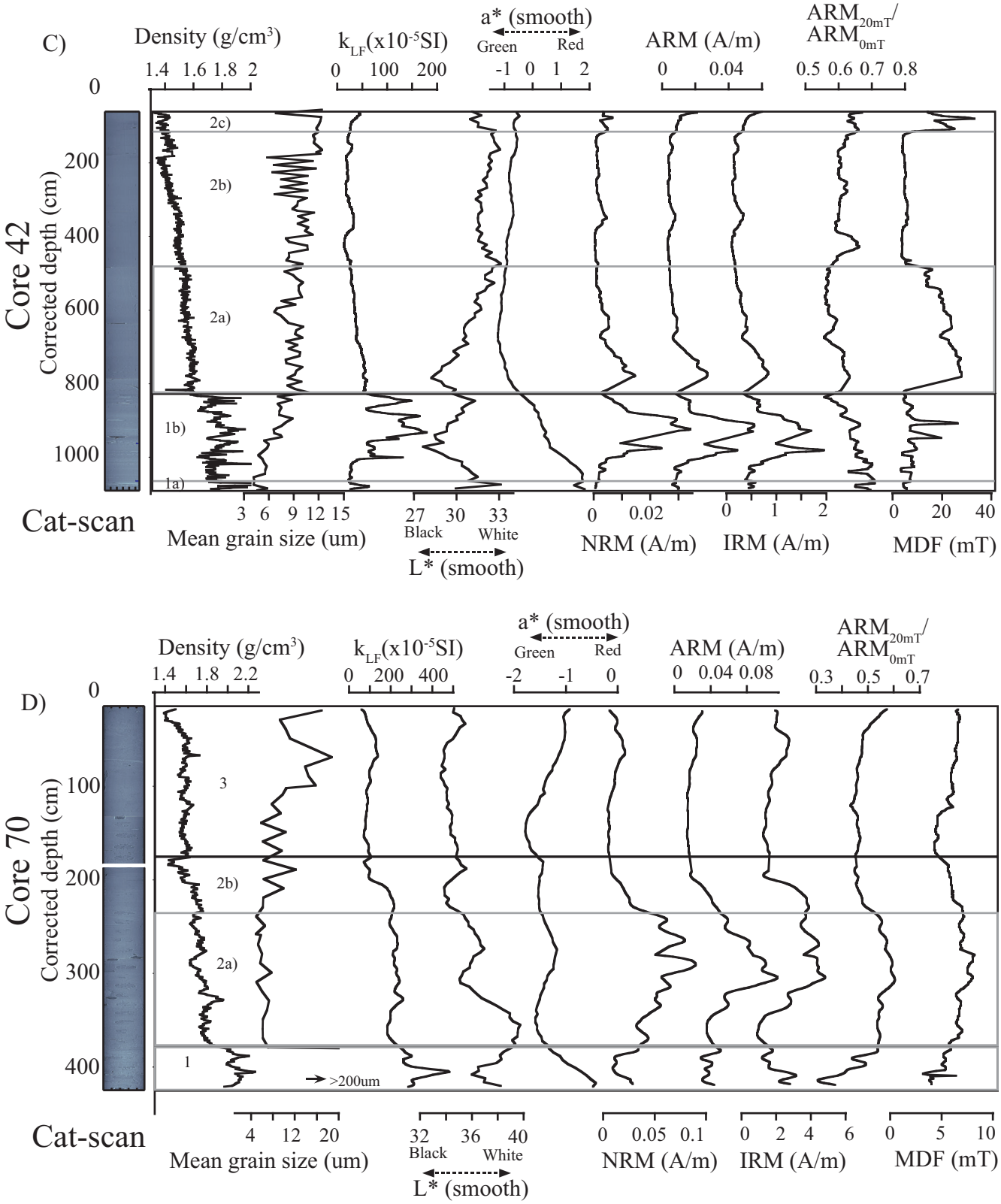

Figure 5. (Continued)

intervals with laminations and normal grading that we interpret as turbidites (also see the CAT-scan images in supporting Figs S1 and S2).

Unit 2, from 835 cm to the top of the core, is composed of very homogeneous and strongly bioturbated olive-grey (5Y4/2) and dark olive-grey (5Y3/2) silty clays. Shell fragments are present at 110 and 80 cm. The sub-units were determined using major changes in the MDF profile. Sub-unit 2a has higher MDF values than sub-unit b, with values ranging from 28 to 14 mT and a decrease starting at 480 cm. Sub-unit c, from 105 to 63 cm, is characterized by relatively higher MDF values with values ranging from 17 and 32 mT.

Core 70

Three units were defined in core 70 (Fig. 5D). The first unit, from 417 to 375 cm, is composed of very dark gray (5Y3/1) sands and contains numerous pebbles and shell fragments. It

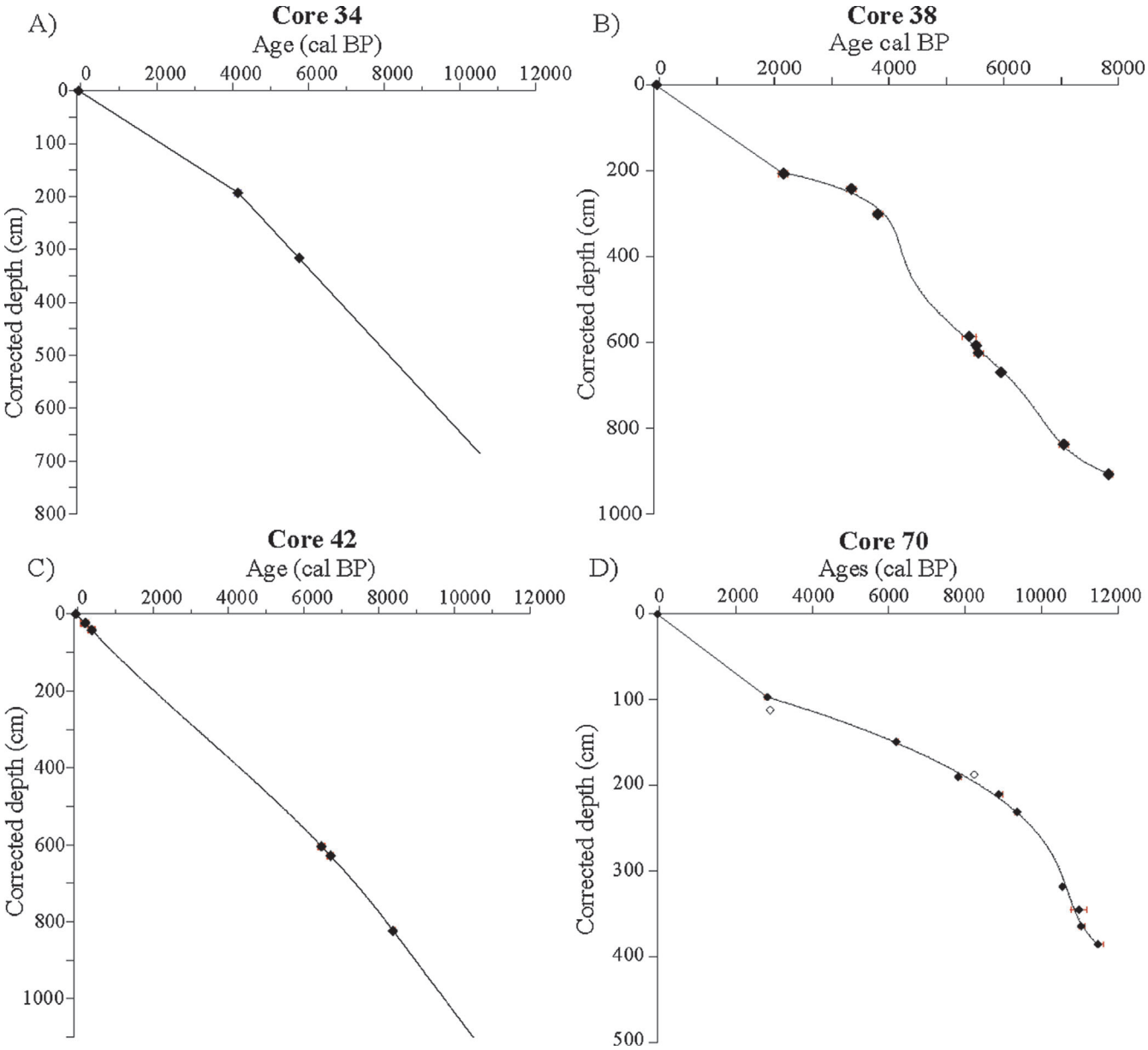

Figure 6. Age model for cores (A) 34, (B) 38, (C) 42 and (D) 70. The depths were corrected for the missing sediments due to piston coring. Error bars reflect the 2σ ranges associated with the calibrated ages. Open symbols illustrate excluded ages.

is associated with a peak in density, mean grain size and magnetic susceptibility. Similarly, very low MDF and ARM_{20mT}/ARM_{0mT} values probably suggest a coarser magnetic grain size (e.g. Andrews *et al.*, 2003; Stoner and St-Onge, 2007), as the hysteresis data reveal a MD magnetic grain size (Fig. 4D).

Unit 2 is observed from 375 to 175 cm. It is characterized by olive (5Y 4/3) and dark olive gray (5Y3/2) silty clays and by relatively high magnetic property values, with magnetic susceptibility reaching values around 200×10^{-5} SI. Sub-unit 2b is a transitional unit to unit 3, with some traces of bioturbation. Toward its top, at 182 cm, there are a few laminations, whereas at the bottom of sub-unit 2a, a few pebbles are observed.

Unit 3 is a homogeneous olive-gray (5Y4/2) silty clay unit with a few traces of bioturbation. From 70 to 60 cm, an interval of higher density is observed on the CAT-scan image. This interval is also characterized by normal grading and an increase in magnetic susceptibility values (max: 140×10^{-5} SI). We interpret this layer as a turbidite. From 45 cm to the top of the core, an increase in a^*, L^* and ARM_{20mT}/ARM_{0mT} is observed.

Chronology

The four radiocarbon-based age models are presented in Fig. 6. Because the four cores have different sedimentation rates and different distributions of ^{14}C ages, four different methods have been used to establish the age models. The age model for core 34 was constructed with a linear interpolation between available ages. There are two different sedimentation rates: 76 cm ka^{-1} from the base to 4000 cal a BP and 46 cm ka^{-1} from 4000 cal a BP to the top of the sequence. The age model for core 38 was constructed using a linear interpolation for the top of the core and a fifth degree polynomial fit for the rest of the core, where several ^{14}C ages were available. The sedimentation rate is 136 cm ka^{-1} for the base of the core, 31 cm ka^{-1} from 2000 to 4000 cal a BP, and 85 cm ka^{-1} for the top of the core. For core 42, the age model was constructed with a simple linear interpolation between all of the calibrated ^{14}C ages. The mean sedimentation rate is 46 cm ka^{-1}. Finally, for core 70, due to the presence of several ^{14}C ages, a fifth degree polynomial fit was established from the base of the core to the uppermost ^{14}C age.

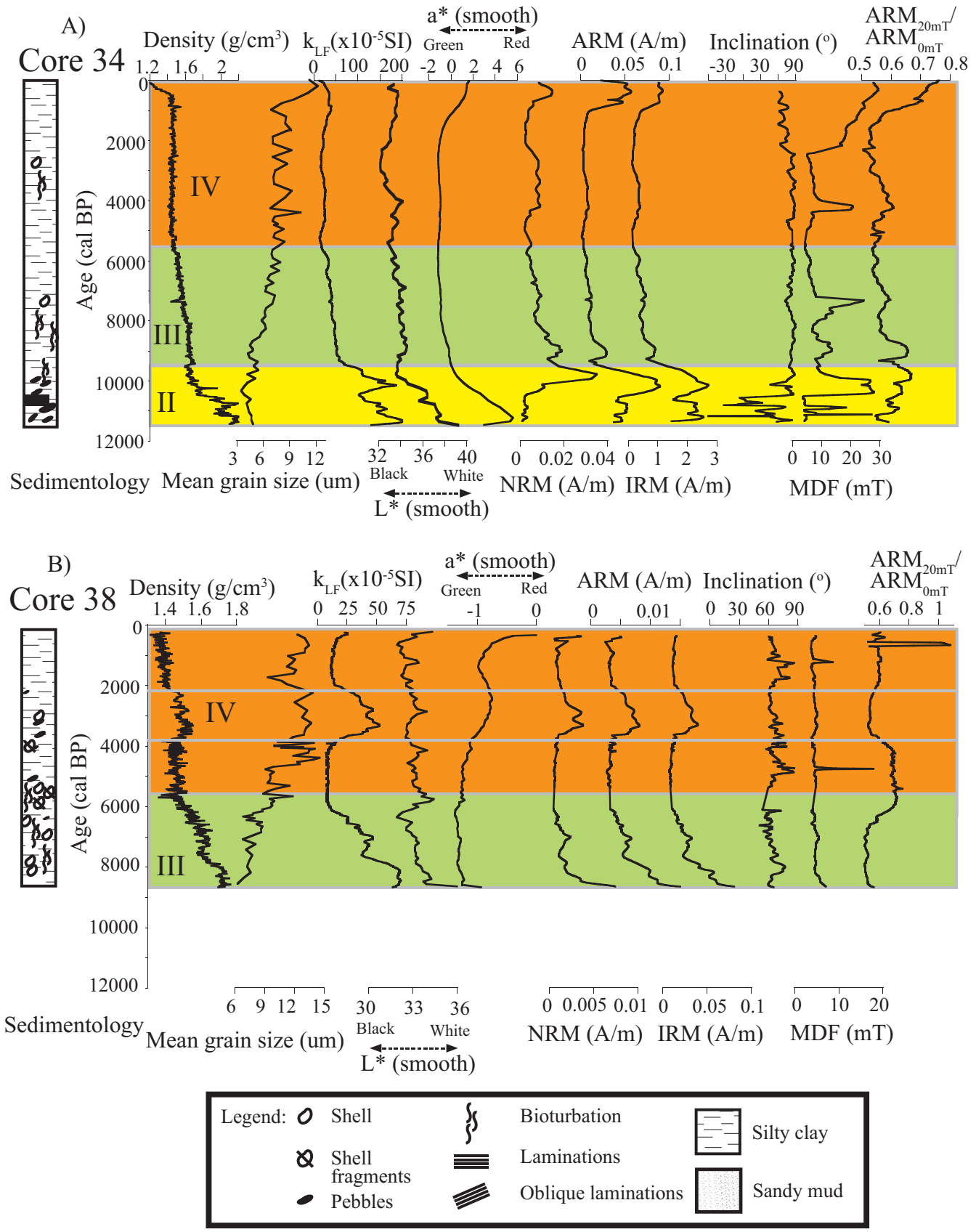

Figure 7. Downcore physical and magnetic properties with the chronostratigraphic units of cores (A) 34, (B) 38, (C) 42 and (D) 70. See text for details. This figure is available in colour online at wileyonlinelibrary.com.

There are two different sedimentation rates for this part of the core: 75 cm ka^{-1} for the base of the core and 20 cm ka^{-1} from ~9000 to ~3000 cal a BP. The top of the age model was constructed using a linear relationship between the first two ages, yielding a sedimentation rate of 32 cm ka^{-1}.

Chronostratigraphic Units and Environmental Changes in Baffin Bay During the Holocene

Chronostratigraphic unit I (12 300–11 300 cal a BP)

Based on the identification and the characteristics of the lithological units observed in each core (Fig. 7), as well as the

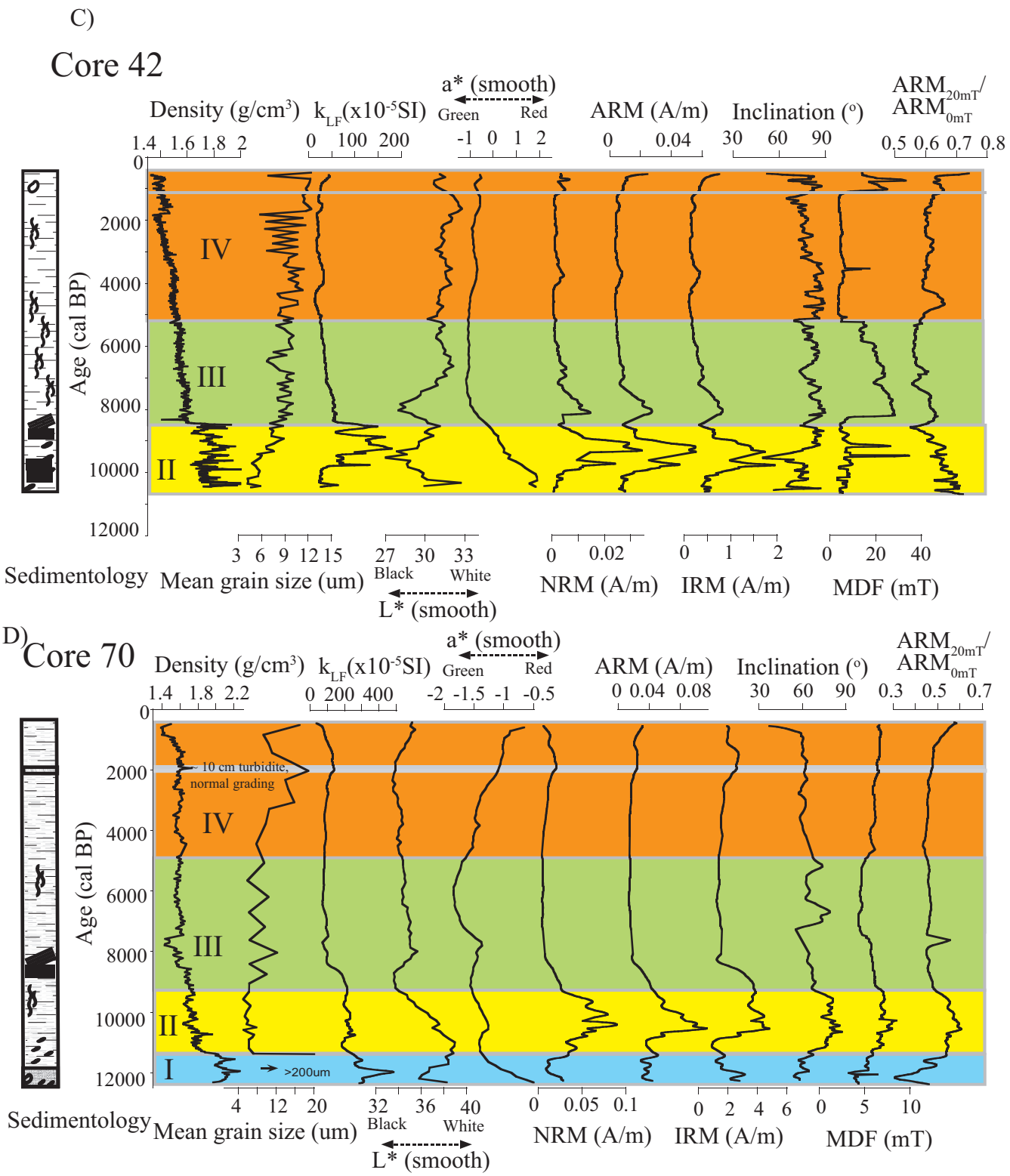

Figure 7. (Continued)

age models, common chronostratigraphic units can be identified between the different cores. The first chronostratigraphic unit (I) is only present in core 70 and is mostly composed of coarse material. It is dated from 12 300 to 11 300 cal a BP. This period corresponds to the transition from the Younger Dryas to the Holocene (12 800–11 700 cal a BP, Funder *et al.*, 2011) and was probably characterized by a significant influx of meltwater (Weidick and Bennike, 2007), as suggested by the sand content, while the presence of pebbles in this facies indicates the passage of icebergs (Stein, 2008). It is interpreted as an ice-proximal glaciomarine sedimentary unit.

According to Ò Cofaigh *et al.* (2013), the limit of the ice margin during the Younger Dryas was at the Fiskebank moraines system, to the east of the sampling site of core 70. But their results show evidence of a glacier outlet in the Outer Egedesminde Dyb, which covered the site of core 70 during the Younger Dryas. The exact timing of the retreat is undated, but Ò Cofaigh *et al.* (2013) determined 12 400 cal a

BP as a maximum age of deglaciation for the outer-shelf trough, which is coherent with the onset of unit 1.

Chronostratigraphic unit II [11 300 to (9400– ~8500) cal a BP]

The second chronostratigraphic unit (II) is present in all cores except core 38 and corresponds mostly to stratigraphic unit 1 for cores 34 and 42, and unit 2a of core 70 (Fig. 5). The presence of pebbles and/or turbidites in the sediment, associated with high magnetic susceptibility values, is an indicator of extensive sea-ice cover or icebergs. In core 34, this unit is characterized by a pronounced red color (a*) associated with lower magnetic remanence values, which reflects the presence of hematite probably transported by glaciers from the Thule Basin (Dawes, 2006).

Moreover, in core 42, the presence of numerous pebbles, sandy mud layers and brownish turbidites in this unit can be linked to large terrigenous inputs from the final collapse of the Innuitian Ice Sheet in the Canadian Arctic Archipelago (Ledu *et al.*, 2010), followed by melting of the Innuitian Ice Sheet on Devon and Ellesmere Islands (England *et al.*, 2006). This unit, interpreted as a diamicton, thus corresponds to the transition from deglaciation to the Holocene Thermal Optimum.

Chronostratigraphic unit III [(9400– ~8500) to (5500–5250) cal a BP]

Chronostratigraphic unit III is present in all cores up to 5500–5250 cal a BP. The unit is associated with stratigraphic unit 1 for core 38 and unit 2 for the other cores. It is characterized by strongly bioturbated silty clays with shells and shell fragments, which suggest a hemipelagic mode of deposition and oceanographic conditions favorable for marine productivity. This corresponds to the Holocene Thermal Optimum for the studied area (Koç and Jansen, 2002; Weidick and Bennike, 2007; Ledu *et al.*, 2010; Jennings *et al.*, 2011). For all cores, the homogeneous fine sediment is interpreted to have a hemipelagic origin, where sedimentation occurred mainly by suspension. This unit shares similarities with a 112-cm layer of highly bioturbated mud described by Jennings *et al.* (2011) in a core from Nares Strait. According to Jennings *et al.* (2011), based on the pervasive bioturbation, as well as the benthic and planktonic foraminifera assemblages, there was high marine productivity between 8926 and 6050 cal a BP in northern Baffin Bay, which is consistent with our results for this unit.

In core 42, the sediments in chronostratigraphic unit III present higher MDF values, which can probably be explained by a finer magnetic grain size as major changes in mineralogy were not recorded by the IRM/SIRM ratio and hysteresis parameters. The MDF profile of the entire core is almost identical to the variations of key paleoceanographic proxies of core HLY03-05GC (Jennings *et al.*, 2011) from Nares Strait (Fig. 8). The relationship between the $\delta^{18}O$ and $\delta^{13}C$ records and MDF is not exactly known, but in previous studies, some links have been established between the dilution of terrigenous material with biogenic sediments and changes in magnetic mineralogy (Brachfeld and Banerjee, 2000; Brachfeld, 2006). In this case, the link between MDF, $\delta^{18}O$ and $\delta^{13}C$ records probably occurs due to the influence of meltwater and the proximity of ice. The meltwater episode before the opening of Nares Strait is associated with warmer surface conditions ($\delta^{18}O$), low marine productivity ($\delta^{13}C$) (Jennings *et al.*, 2011) and coarser terrigenous material (lower MDF values). The Holocene Climatic Optimum is then characterized by the occurrence of finer sediment due to

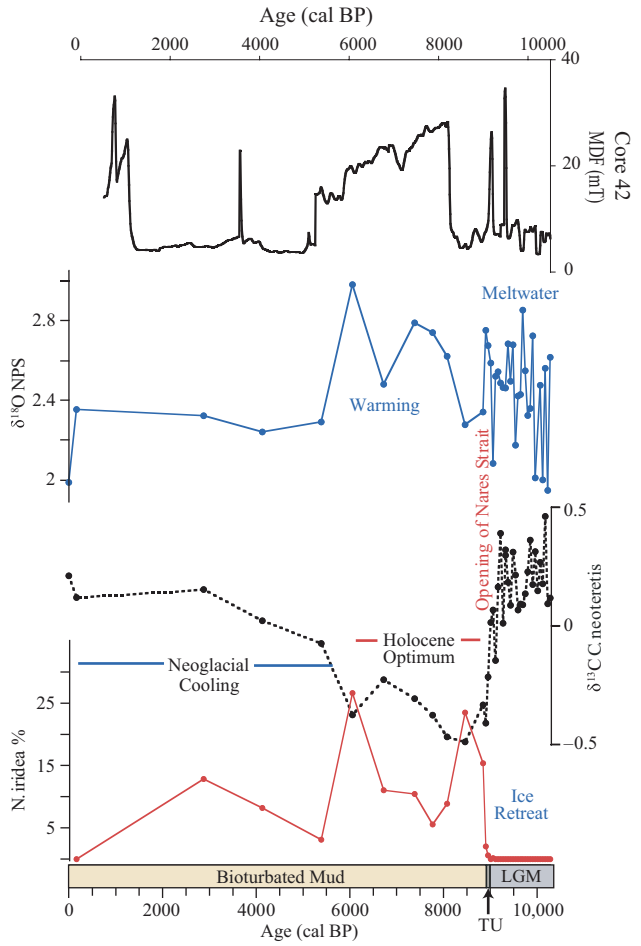

Figure 8. Comparison between the MDF profile of core 42 and key paleoceanographic proxies of core HLY03-05GC from Jennings *et al.* (2011). TU, the transitional unit associated with the opening of Nares Strait observed in core HLY03-05GC. LGM, Last Glacial Maximum. This figure is available in colour online at wileyonlinelibrary.com.

hemipelagic sedimentation, which results in higher MDF values and high marine productivity ($\delta^{13}C$). Similarly, the k_{ARM} versus k_{LF} diagram (Banerjee *et al.*, 1981; King *et al.*, 1982) indicates finer magnetic grains during this time interval. The k_{ARM} versus k_{LF} diagram (Banerjee *et al.*, 1981; King *et al.*, 1982) has established that the magnetic grain size was finest during the Holocene Climatic Optimum (Fig. 9) even though the values from this diagram should not be taken as absolute values for several reasons, namely that the diagram is based on laboratory assemblages rather than natural magnetite samples (King *et al.*, 1982), and that the ARM depends on the experimental process by which the remanence is imparted (Sagnotti *et al.*, 2003).

For core 70, the onset of this chronostratigraphic unit is concomitant with the establishment of the WGC in the bay between 9200 and 7800 cal a BP (Lloyd *et al.*, 2005). The increase in sea surface temperatures for the south-eastern part of Baffin Bay during the thermal maximum is caused by the influence of the WGC on meltwater from the Jakobshavn Isbrae ice stream and local glaciers from Disko Island (Lloyd *et al.*, 2005; Kelly and Lowell, 2009). The transition in the sedimentation rates is around 8800 cal a BP (Fig. 6).

Figure 10 illustrates the comparison between the density and k_{LF} profiles and two temperature profiles from the Greenland Ice Core Project (GRIP) borehole (Dahl-Jensen *et al.*, 1998), as well as a compilation from ice-core records in Greenland (Weidick and Bennike, 2007). Overall, this correlation can be explained by the fact that variations in

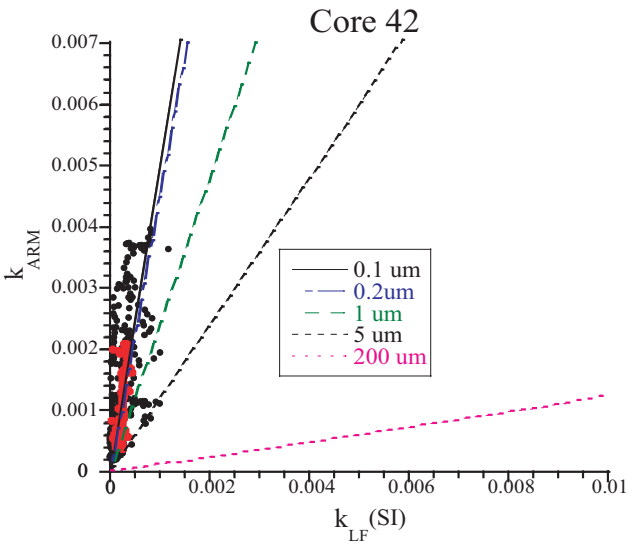

Figure 9. k_{ARM}/k_{LF} diagram for core 42. Symbols in red are for the 8250–6000 cal a BP interval. See text for details. This figure is available in colour online at wileyonlinelibrary.com.

continental temperatures directly affect the presence, or absence, of meltwater and sea ice inputs in Disko Bay, and thereby the density and magnetic susceptibility of the sediment.

Chronostratigraphic unit IV (5500–5250 cal a BP to present)

The most recent chronostratigraphic unit (IV) mostly corresponds to lithostratigraphic units 2 and 3. The unit is characterized by a slight augmentation in mean grain size. A similar increase was also observed in a core (012P) from Smith Sound (Knudsen *et al.*, 2008) and interpreted as an increase in Arctic bottom currents during this period (Knudsen *et al.*, 2008). On the other hand, this change in grain size could also be caused by increased erosion in the area due to local glacier activity on land from 5710 cal a BP to the present (5053 corrected a ^{14}C BP, Jennings, 1993). However, this slight increase is not associated with an increase in magnetic susceptibility, which normally occurs with a contribution of terrigenous material (Andrews and Jennings, 1987, 1990; Stoner *et al.*, 1996).

Unit IV contains significantly less traces of bioturbation than the underlying unit, which could be an indication of colder conditions. In addition, in core 38 a major peak in k_{LF} at 3300 a cal BP is caused by the presence of pebbles, which probably indicates deposition by iceberg calving and thus supports a cold event in the area. This event was also identified by Wanner *et al.* (2011) and Bond *et al.* (1997) between 3300 and 2500 cal a BP and at 2800 cal a BP, respectively, in the North Atlantic. A cool and unstable environment from 3050 to 2550 cal a BP was also observed by Knudsen *et al.* (2008) in a core (008P) located near core 38 in Smith Sound.

Core 70 contains a 10-cm-thick turbidite at ~1885 cal a BP (Fig. 7D). This turbidite could have been deposited following an intense episode of iceberg rafting, determined by Andresen *et al.* (2010) to have occurred in Disko Bugt at 2100 cal a BP. This may have been triggered by the onset of the Roman Warm Period in Europe (Perner *et al.*, 2011), which followed a period of colder conditions from 3600 to 1900 cal a BP (Perner *et al.*, 2011). Following these colder conditions, a warmer WGC was observed which would have caused an increase in meltwater outflow and iceberg calving (Lloyd *et al.*, 2005; Moros *et al.*, 2006; Andresen *et al.*, 2010).

Conclusions

The main chronostratigraphic units from the four cores reflect major Holocene environmental changes in Baffin Bay. Variations in magnetic grain size and concentration, as well as

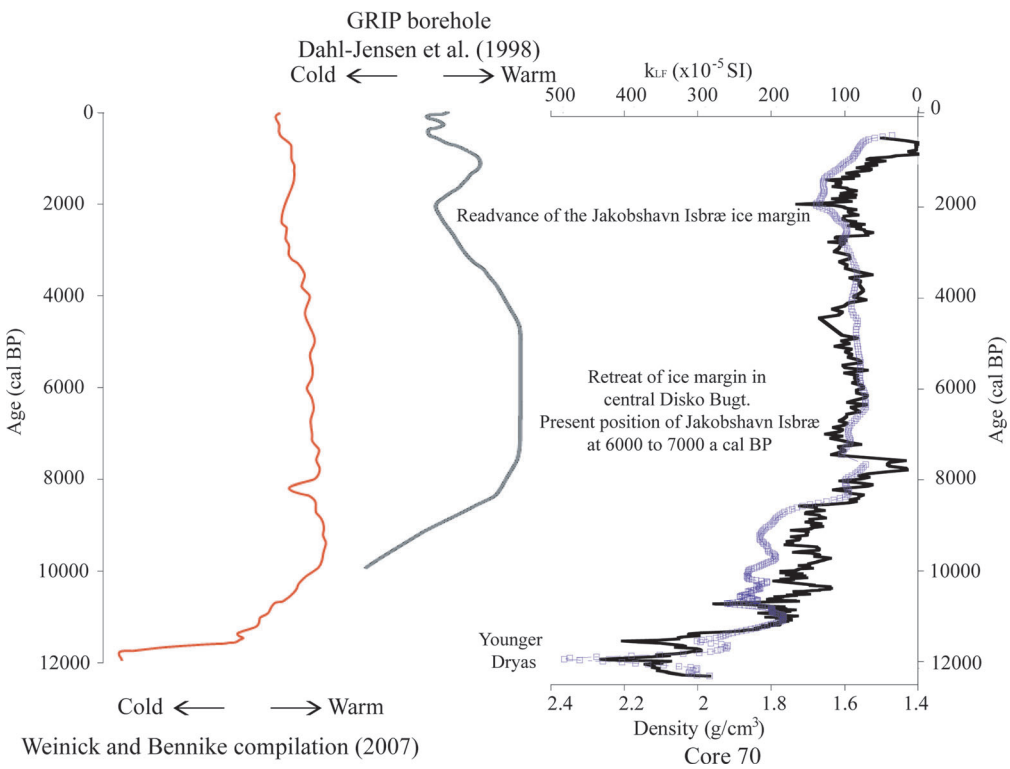

Figure 10. Comparison of the magnetic susceptibility (blue squares) and density (black line) profiles of core 70 with temperature profiles from Weidick and Bennike (2007) and Dahl-Jensen *et al.* (1998) (ice cores). This figure is available in colour online at wileyonlinelibrary.com.

changes in physical properties such as grain size, color and density, are indicative of environmental changes. Cores 34, 42 and 70 recorded the transition from the Younger Dryas to the Holocene, marked by the presence of diamicton, ice-rafted debris and turbidites, as well as the Holocene Climatic Optimum, indicated by very fine hemipelagic and highly bioturbated sediment. The MDF_{NRM} signal of core 42, as well as density and k_{LF} for core 70, are good proxies of environmental changes as they are related to changes in grain size. Finally, signatures of local events were identified during the Neoglacial period. Indeed, core 38 from northern Baffin Bay has a specific signal of ice-rafted debris and coarse grains marking a cold event from 2500 to 3300 cal a BP, while core 70 contains a turbidite dated at ~1885 cal a BP that is probably associated with local iceberg calving generated by warmer WGC waters at that time (Moros *et al.*, 2006; Andresen *et al.*, 2010; Perner *et al.*, 2011). These data show overall paleoceanographic variations in Baffin Bay during the Holocene and some local climatic events during the Neoglacial period.

Supporting Information

Additional supporting information can be found in the online version of this article:

Figure S1. Background_dataset_cores34_38.
Figure S2. Background_dataset_cores42_70.

Acknowledgements. We are grateful to the captain, officers, crew and scientists on board the CCGS *Hudson* during the 2008-029 expedition, funded by the Geological Survey of Canada and the Natural Sciences and Engineering Research Council of Canada (NSERC). This study was supported by the Fonds Québécois de recherche en Nature et Technologies, NSERC, the Economic Development, Innovation and Export Trade Ministry of Quebec (Canadian contribution to the Past4Future project) and the Canadian Foundation for Climate and Atmospheric Sciences (CFCAS). We thank Nicolas Van Nieuwenhove and two anonymous reviewers for their thorough reviews and helpful comments. We also sincerely thank Anne Jennings (INSTAAR) for sharing the ^{14}C dates of core 70 and for commenting on a preliminary version of the manuscript. We also thank Joseph Ortiz (Kent State University) for the diffuse spectral reflectance measurements.

Abbreviations. AF, alternating field; AMS, accelerator mass spectrometry; ARM, anhysteretic remanent magnetization; BC, box core; DC, direct current; Hc, coercivity; Hcr, coercivity of remanence; IRM, isothermal remanent magnetization; MD, multi-domain; MDF, median destructive field; Mrs, saturation remanence; Ms, saturation magnetization; NRM, natural remanent magnetization; PC, piston core; PSD, pseudo-single domain; SIRM, saturated isothermal remanent magnetization; TWC, trigger weight core; WGC, West Greenland Current.

References

Aksu AE, Piper DJW. 1987. Late Quaternary sedimentation in Baffin Bay. *Canadian Journal of Earth Science* **24**: 1833–1846.

Andersen OGN. 1981. The annual cycle of temperature, currents and water masses in Disko Bugt and adjacent waters, West Greenland. *Meddelelser om Grønland. Bioscience* **5**: 1–36.

Andresen C, David JS, McCarthy C, *et al.* 2010. Interaction between subsurface ocean waters and calving of the JakobshavnIsbræ during the late Holocene. *The Holocene* **21**: 221–224.

Andrews JT, Hardadottir J, Stoner JS. 2003. Decadal to millennial-scale periodicities in North Iceland shelf sediments over the last 12 000 cal yr: long-term North Atlantic oceanographic variability and solar forcing. *Earth and Planetary Science Letters* **210**: 453–465.

Andrews JT, Jennings AE. 1987. Influence of sediment source and type on the magnetic susceptibility of fiord and shelf deposits, Baffin Island and Baffin Bay, N.W.T. *Canadian Journal of Earth Sciences* **24**: 1386–1401.

Andrews JT, Jennings AE. 1990. Geomagnetic secular variations (inclination) of high latitude fiord cores: eastern Canadian Arctic. *Polar Research* **8**: 245–259.

Banerjee SK, King J, Marvin J. 1981. A rapid method for magnetic granulometry with applications to environmental studies. *Geophysical Research Letters* **8**: 333–336.

Blott SJ, Pye K. 2001. Gradistat: a grain size distribution and statistics package for the analysis of unconsolidated sediments. *Earth Surface Processes and Landforms* **26**: 1237–1248.

Bond G, Showers W, Cheseby M, *et al.* 1997. A pervasive millennial-scale cycle in the North Atlantic Holocene and glacial climates. *Science* **294**: 2130–2136.

Brachfeld SA. 2006. High-field magnetic susceptibility (χHF) as a proxy of biogenic sedimentation along the Antarctic Peninsula. *Physics of the Earth and Planetary Interiors* **156**: 274–282.

Brachfeld SA, Banerjee SK. 2000. Rock-magnetic carriers of century-scale susceptibility cycles in glacial marine sediments from the Palmer Deep, Antarctic Peninsula. *Earth and Planetary Science Letters* **176**: 443–455.

Dahl-Jensen D, Mosegaard K, Gundestrup N, *et al.* 1998. Past temperatures directly from the Greenland Ice Sheet. *Science* **282**: 268–271.

Dankers P. 1981. Relationship between median destructive field and remanent coercive forces for dispersed natural magnetite, titanomagnetite and hematite. *Geophysical Journal of the Royal Astronomical Society* **64**: 447–461.

Day R, Fuller M, Schmidt VA. 1977. Hysteresis properties of titanomagnetite: grain-size and compositional dependence. *Physics of the Earth and Planetary Interiors* **13**: 260–267.

Dawes PR. 2006. Explanatory notes to the Geological map of Greenland, 1:500 000, Thule, Sheet 5. *Geological Survey of Denmark and Greenland, Map Series* **2**.

Dearing J. 1999. *Environmental Magnetic Susceptibility: Using the Bartington MS2 System*. Chi Publishing: Kenilworth, UK.

Dunlop DJ. 2002. Theory and application of the Day plot (Mrs/Ms versus Hcr/Hc) 2. Application to data for rocks, sediments, and soils. *Journal of Geophysical Research* **107**: 5/1–5/15.

England JH, Atkinson N, Bednarski JB, *et al.* 2006. The Innuitian Ice Sheet: configuration, dynamics and chronology. *Quaternary Science Reviews* **25**: 689–703.

Francus P (ed.). 2004. *Image Analysis, Sediments, and Paleoenvironmental Reconstructions*. Kluwer: Dordrecht.

Funder S, Kjeldsen KK, Kjær KH, *et al.* 2011. The Greenland Ice Sheet during the past 300,000 years: a review. In *Quaternary Glaciations: Extent and Chronology, Developments in Quaternary Science 15*, Ehlers J, Gibbard PL (eds). Elsevier: Amsterdam; 699–713.

Holland MM, Bitz CM, Eby M, *et al.* 2001. The role of ice–ocean interactions in the variability of the North Atlantic thermohaline circulation. *Journal of Climate* **14**: 656–675.

Hughen KA, Baillie MGL, Bard E, *et al.* 2004. Marine04 marine radiocarbon age calibration, 26-0 ka BP. *Radiocarbon* **46**: 1059–1086.

Jennings AE. 1993. The Quaternary history of Cumberland Sound, southeastern Baffin Island: the marine evidence. *Géographie physique et Quaternaire* **47**: 21–42.

Jennings AE, Sheldon C, Cronin TM, *et al.* 2011. The Holocene history of Nares Strait: transition from glacial bay to Arctic–Atlantic throughflow. *Oceanography* **24**: 26–41.

Jennings AE, Walton ME. 2010. Reconstruction of Early Holocene West Greenland Ice Sheet and West Greenland Current using radiocarbon dating and foraminiferal assemblages. In The State of the Arctic Conference, Miami, FL. Poster.

Jennings AE, Walton ME, O'Cofaigh C, *et al.* 2013. Paleoenvironments during Younger Dryas – Early Holocene Greenland Ice Sheet retreat from outer Disko Trough, central west Greenland. *Journal of Quaternary Science*, this issue.

Kelly MA, Lowell TV. 2009. Fluctuations of local glaciers in Greenland during latest Pleistocene and Holocene time. *Quaternary Science Reviews* **28**: 2088–2106.

King J, Banerjee SK, Marvin J, *et al.* 1982. A comparison of different magnetic methods for determining the relative grain size of magnetite in natural materials: some results from lake sediments. *Earth and Planetary Science Letters* **59**: 404–419.

Knudsen KL, Stabell B, Seidenkrantz MS, *et al*. 2008. Deglacial and Holocene conditions in northernmost Baffin Bay: sediments, foraminifera, diatoms and stable isotopes. *Boreas* **37**: 346–376.

Koç N, Jansen E. 2002. Holocene climate evolution of the North Atlantic Ocean and the Nordic Seas- a synthesis of new results. In *Climate Development and History of the North Atlantic Realm*, Wefer G, Berger WH, Behre KE, Jansen E (eds). Springer: Berlin; 165–173.

Krawczyk D, Witkowski A, Moros M, *et al*. 2010. Late-Holocene diatom-inferred reconstruction of temperature variations of the West Greenland Current from DiskoBugt, central West Greenland. *The Holocene* **20**: 659–666.

Ledu D, Rochon A, de Vernal A, *et al*. 2010. Holocene paleoceanography of the Northwest Passage, Canadian Arctic Archipelago. *Quaternary Science Reviews* **29**: 3468–3488.

Levac E, de Vernal A, Blake WJ. 2001. Sea-surface conditions in northernmost Baffin Bay during the Holocene: palynological evidence. *Journal of Quaternary Science* **16**: 353–363.

Lisé-Pronovost A, St-Onge G, Brachfeld S, *et al*. 2009. Paleomagnetic constraints on the Holocene stratigraphy of the Arctic Alaskan margin. *Global and Planetary Change* **68**: 85–99.

Lloyd JM. 2006. Late Holocene environmental change in DiskoBugt, west Greenland: interaction between climate, ocean circulation and JakobshavnIsbrae. *Boreas* **35**: 35–49.

Lloyd JM, Parka LA, Kuijpers A, *et al*. 2005. Early Holocene palaeoceanography and deglacial chronology of Disko Bugt, West Greenland. *Quaternary Science Reviews* **24**: 1741–1755.

Mazaud A. 2005. User-friendly software for vector analysis of the magnetization of long sediment cores. *Geochemistry Geophysics Geosystems* **6**: Q12006.

Melling H, Gratton Y, Ingram G. 2001. Ocean circulation within the North Water polynya of Baffin Bay. *Atmosphere-Ocean* **39**: 301–325.

Miller GH, Wolfe AP, Briner JP, *et al*. 2005. Holocene glaciations and climate evolution of Baffin Island, Arctic Canada. *Quaternary Science Review* **24**: 1703–1721.

Moros M, Jensen KG, Kuijpers A. 2006. Mid- to late-Holocene variability in Disko Bugt, central West Greenland. *The Holocene* **16**: 357–367.

Ó Cofaigh C, Dowdeswell JA, Jennings AE, *et al*. 2013. An extensive and dynamic ice sheet on the West Greenland shelf during the last glacial cycle. *Geology* **41**: 219–222.

Perner K, Moros M, Lloyd JM, *et al*. 2011. Centennial scale benthic foraminiferal record of late Holocene oceanographic variability in Disko Bugt, West Greenland. *Quaternary Science Reviews* **30**: 2815–2826.

Peters C, Dekkers MJ. 2003. Selected room temperature magnetic parameters as a function of mineralogy, concentration and grain size. *Physics and Chemistry of the Earth* **28**: 659–667.

Ribergaard MH, Olsen SM, Mortensen J. 2008. Oceanographic Investigations off West Greenland 2007, NAFO SCR Doc. 08/3, Scientific Council Meeting – June 2008. Danish Meteorological Institute Centre for Ocean and Ice; Copenhagen, Denmark.

Roberts AP. 2006. High-resolution magnetic analysis of sediment cores: strengths, limitations and strategies for maximizing the value of long-core magnetic data. *Physics of the Earth and Planetary Interiors* **156**: 162–178.

Sagnotti L, Rochette P, Jackson M, *et al*. 2003. Inter-laboratory calibration of low field and anhysteretic susceptibility measurements. *Physics of the Earth and Planetary Interiors*, **138**: 25–38.

Stein R. 2008. *Arctic Ocean Sediments: Processes, Proxies, and Palaeoenvironment*, Developments in Marine Geology, Vol. 2. Elsevier: Amsterdam.

Stoner JS, Channell JET, Hillaire-Marcel C. 1996. The magnetic signature of rapidly deposited detrital layers from the deep Labrador Sea: relationship to North Atlantic Heinrich layers. *Paleoceanography* **11**: 309–325.

Stoner JS, St-Onge G. 2007. Magnetic stratigraphy in paleoceanography: reversals, excursions, paleointensity, and secular variation in proxies. In *Late Cenozoic Paleoceanography, Developments in Marine Geology*, Hillaire-Marcel C, De Vernal A (eds). Elsevier: Amsterdam; 99–137.

St-Onge G, Chapron E, Mulsow S, *et al*. 2012. Comparison of earthquake-triggered turbidites from the Saguenay (Eastern Canada) and Reloncavi (Chilean margin) Fjords: implications for paleoseismicity and sedimentology. *Sedimentary Geology* **243–244**: 89–107.

St-Onge G, Mulder T, Francus P, *et al*. 2007. Continuous physical properties of cored marine sediments. In *Proxies in Late Cenozoic Paleoceanography*, Hillaire-Marcel C, De Vernal A (eds). Elsevier: Amsterdam; 63–98.

St-Onge G, Piper DJW, Mulder T, *et al*. 2004. Earthquake and flood-induced turbidites in the Saguenay Fjord (Québec): a Holocene paleoseismicity record. *Quaternary Science Reviews* **23**: 283–294.

Stuiver M, Polach HA. 1977. Discussion: reporting of ^{14}C data. *Radiocarbon* **19**: 355–363.

Stuiver M, Reimer PJ, *et al*. 2005. CALIB 5.0. Available from http://radiocarbon.pa.qub.ac.uk/calib/.

Tang CCL, Ross CK, Yao T, *et al*. 2004. The circulation, water masses and sea-ice of Baffin Bay. *Progress in Oceanography* **63**: 183–228.

Tauxe L. 1993. Sedimentary records of relative paleointenisty of the geomagnetic field in sediments: theory and practice. *Reviews of Geophysics* **31**: 319–354.

Tauxe L. 2010. *Essentials of Paleomagnetism*. University of California Press: Los Angeles.

Thompson R, Oldfield F. 1986. *Environmental Magnetism*. George Allen and Unwin: London.

Wanner H, Solomina O, Grosjean M, *et al*. 2011. Structure and origin of Holocene cold events. *Quaternary Science Reviews* **30**: 3109–3123.

Weeks R, Laj C, Endignoux L, *et al*. 1993. Improvements in long-core measurement techniques: applications in palaeomagnetism and palaeoceanography. *Geophysical Journal International* **114**: 651–662.

Weidick A, Bennike O. 2007. Quaternary glaciation history and glaciology of JakobshavnIsbræ and the DiskoBugt region, West Greenland: a review. In Geological Survey of Denmark and Greenland Bulletin 14. Geological Survey of Denmark and Greenland: Copenhagen, Denmark; 1–13 and 26–49.

